Biosensors and Bioelectronics 145 (2019) 111672

Contents lists available at ScienceDirect

Biosensors and Bioelectronics

journal homepage: www.elsevier.com/locate/bios

A nitrile-mediated aptasensor for optical anti-interference detection of acetamiprid in apple juice by surface-enhanced Raman scattering

Yue Sun[a,1], Zhihua Li[a,1], Xiaowei Huang[a], Di Zhang[a], Xiaobo Zou[a,*], Jiyong Shi[a,**], Xiaodong Zhai[a], Caiping Jiang[a], Xiaoou Wei[a], Tingting Liu[b]

[a] Agricultural Product Processing and Storage Lab, School of Food and Biological Engineering, Jiangsu University, Zhenjiang, Jiangsu, 212013, China
[b] School of Chemistry and Chemical Engineering, Jiangsu University, Zhenjiang, Jiangsu, 212013, China

ARTICLE INFO

Keywords:
Optical anti-interference
Acetamiprid
Surface-enhanced Raman scattering
Aptasensor
AgNPs@Si

ABSTRACT

Currently, the detection of pesticide is critical for food safety assurance, but it is still challenging due to the presence of biological interferents from complex food matrix. In this study, we developed an optical anti-interference surface-enhanced Raman scattering (SERS) aptasensor system for trace detection of acetamiprid. 4-(Mercaptomethyl) benzonitrile (MMBN) containing C≡N bond was used as Raman tag to provide a sharp peak (2227 cm^{-1}) in the Raman-silent spectral window (1800-2800 cm^{-1}) where no Raman signal existed for most of molecules. Gold nanoparticles (AuNPs) bonded with polyadenine (polyA)-mediated aptamer and Raman tag (MMBN-AuNPs-aptamer) was synthesized as Raman probe, while the complementary DNA (cDNA) conjugated with AgNPs-decorated silicon wafer (AgNPs@Si) was used as SERS substrate. As acetamiprid molecule could specifically combine with aptamer, preventing the formation of MMBN-AuNPs-aptamer-cDNA-AgNPs@Si (expressed as "Au-AgNPs@Si") hybrid through DNA sequence linking, Raman signal intensities of MMBN in Au-AgNPs@Si decreased when the concentration of acetamiprid increased. Under the optimum assay condition, the proposed method displayed a linear response for acetamiprid detection in the range of 25–250 nM with a low detection limit of 6.8 nM. Finally, the developed aptasensor was successfully used to determine acetamiprid content in apple juice. Accordingly, this novel anti-interference SERS aptasensor could be a promising acetamiprid sensor for food safety assurance.

1. Introduction

China is the largest apple juice producer and exporter in the world (Juan et al., 2013). The safety and quality of apple juice are the most important considerations for manufacturers and consumers. Acetamiprid, as a highly efficient broad-spectrum insecticide, has been commonly used for pest control since 1995 (Renaud et al., 2018). Considering its wide, frequent and extensive use, acetamiprid would remain in soil and be washed from farmland into river by rain (Pramanik et al., 2006; Sanyal et al., 2008). Therefore, acetamiprid would inevitably accumulate in sprayed food such as apple. Despite its low toxicity to mammalian, acetamiprid was associated with endocrine system disruption (Albanito et al., 2008), carcinogenesis (Tchounwou et al., 2001) and birth defects (Cooper et al., 2007). Therefore, the selective and sensitive detection of acetamiprid in apple juice is crucial for human health.

To date, acetamiprid residues was mainly detected based on standard analytical methods such as high performance liquid chromatography (HPLC) (Xie et al., 2011), gas chromatography (GC) (Zhang et al., 2008), mass spectrometry (MS) (Park et al., 2011) and enzyme-linked immunosorbent assays (ELISA) (Kim et al., 2004). Although these methods own the distinctive superiority of high accuracy and sensitivity, they require expensive instruments, trained personnel and are not suitable for on-site testing. Alternatively, other methods such as colorimetric (Yang et al., 2015), electrochemical (Rapini et al., 2016), fluorescent (Jung et al., 2007; Liu et al., 2016) and surface-enhanced Raman spectroscopy (SERS) combining with nano-biotechnology (Wang et al., 2010) have been developed for the detection of pesticides due to the advantages of simplicity, sensitivity and noninvasiveness. Among these methods, SERS has been proven to be a promising tool for biomolecules detection in various fields, including living cells imaging (Cheng et al., 2017; Li et al., 2015a), public security (Jamil et al.,

* Corresponding author.
** Corresponding author.
E-mail addresses: zou_xiaobo@ujs.edu.cn (X. Zou), shi_jiyong@ujs.edu.cn (J. Shi).
[1] these authors contributed equally to this work.

https://doi.org/10.1016/j.bios.2019.111672
Received 1 April 2019; Received in revised form 15 August 2019; Accepted 2 September 2019
Available online 03 September 2019
0956-5663/ © 2019 Published by Elsevier B.V.

2015), food safety (Han et al., 2017), and environmental monitoring (Fu et al., 2015) by virtue of its intrinstic advantages such as excellent fingerprint identification, high sensitivity, and less time-consuming process. Nevertheless, there is still some problems remaining to solve for practical application, especially for food detection (Li et al., 2015b; Liu et al., 2011; Zhao et al., 2014). One of the most outstanding one is the optical interferences caused by spectral stacking between inherent biomolecules in food organics and the SERS-readout probes (Wang et al., 2013), which would inevitably impact the detection accuracy (Sun et al., 2015). Thus, it is still challenging to develop novel Raman probes resisting to interference from organic biomolecules.

Recently, Hu et al. (2018) and Wei et al. (2014) reported that alkyne or nitrile (that is, C≡C or C≡N) moiety displayed distinct and sharp Raman scattering peaks in the Raman-silent spectral window (1800–2800 cm^{-1}) (Yamakoshi et al. 2011, 2012), where no Raman signals exist for most biomolecules. Owing to its minimal optical interferences and super sensitivity, alkyne and nitrile have been utilized in screening and identification of small molecules such as proteins, antigens, fatty acids and thymidine analogues in living cells, coupling with SERS spectroscopy (Ando et al., 2016; Chen et al., 2016; Zhang et al., 2018). Moreover, based on the cysteine (C)–Ag^{+}-C and thymidine (T)-Hg^{2+}-T coordination, Zeng et al. (2016) succeeded in heavy-metal ions detection impervious to spectral interferences in organic pollutants by employing alkyne-derivatives as Raman tags. However, these alkyne/nitrile-functionalized Raman tags have not been applied to detect pesticide molecule in complex food organic media.

In this work, we designed a nitrile-functionalized aptasensor for optical anti-interference detection of acetamiprid. As illustrated in Scheme 1, the aptasensor system was designed based on AuNPs linked with aptamer and Raman tag (MMBN-AuNPs-aptamer), as well as AgNPs@Si substrates conjugated with cDNA (cDNA-AgNPs@Si). By utilizing the specific molecular interaction between acetamiprid and aptamer, AuNPs with Raman tag cannot be connected with AgNPs@Si substrate through DNA sequence linking. Consequently, Raman intensity of MMBN on substrate linearly reduced with the addition of acetamiprid. Hence the Raman intensity of MMBN on Au-AgNPs@Si were inversely proportional to the amount of acetamiprid. There are two typical advantages for our SERS aptasensor: First, the utilization of MMBN as Raman tag could avoid spectral stacking interferences in presence of other organics; Second, by using polyA-mediated aptamer, the monovalent DNA-gold nanoparticles (mDNA-AuNP) can be formed in a facile and purification-free way, which offers a better control of monovalent DNA assembly on AuNPs surface compared to the functionalization of thiolated DNA onto AuNPs (Wang et al., 2014; Yao et al., 2015).

2. Materials and methods

2.1. Chemicals and reagents

Acetone, sulphuric acid (H_2SO_4) (99%), hydrogen peroxide (H_2O_2), hydrofluoric acid (HF) (40%), silver nitrate ($AgNO_3$), chlorauric acid ($HAuCl_4$) and trisodium citrate were purchased from Sinopharm Chemical Reagent Co., Ltd (China). 4-(Mercaptomethyl) benzonitrile (MMBN) was obtained from Sigma-Aldrich (USA). Acetamiprid, imidacloprid, dichlorvos, phoxim, malathion and profenofos were purchased from Aladdin Chemistry Co., Ltd. A phosphate-doped (p-type) silicon wafer (ρ = 0.01–0.02 Ω cm) was purchased from Shunsheng Electronic Technology Co., Ltd (China). Other reagents were all analytical grade and applied as received without further purification.

DNA oligonucleotide of the acetamiprid-binding aptamer (5′-AAAAA CTGAC ACCAT ATTAT GAAGA -3′) and the complementary DNA (cDNA) (5′- (SH) - $(CH_2)_6$ - TCTTC ATAAT ATGGT GTCAG - 3′) were synthesized and purified by Sangon Biotechnology (Shanghai, China). Double-distilled water was used in all experiments.

2.2. Apparatus

The field emission scanning electron microscopy (SEM) (JSM-7001F, JEOL Ltd, Tokyo, Japan) setting at 15.0 kV acceleration voltage was used for characterization of as-prepared AgNPs@Si substrate and Au-AgNPs@Si. An attached energy-dispersive X-ray (EDX) spectroscopy facility in the SEM was applied to chemical composition analysis. High resolution transmission electron microscope (JEM-2100, JEOL Ltd., Tokyo, Japan) (TEM) was conducted with the operation voltage at 200 kV to observe the morphology of AuNPs. The SERS analysis was performed on a confocal laser-Raman spectrometer (DXR, Thermo Fisher Ltd, USA) equipment with excitation of 532 nm. The wavenumber accuracy of the instrument is less than 2 cm^{-1}.

2.3. Synthesis of AgNPs@Si substrate

The process of AgNPs deposition on silicon wafer (AgNPs@Si) was carried out according to previous literatures (Dao et al., 2016; Haldar et al., 2014). At first, a Si wafer was cleaned with acetone by ultrasound for 10 min to remove grease, and rinsed with double-distilled water. The wafer was then cleaned with H_2SO_4–H_2O_2 (3:1, v/v) for 30 min and washed by double-distilled water. Next, the cleaned wafer was immersed in HF (5%) solution for 30 min to form the H-terminated Si

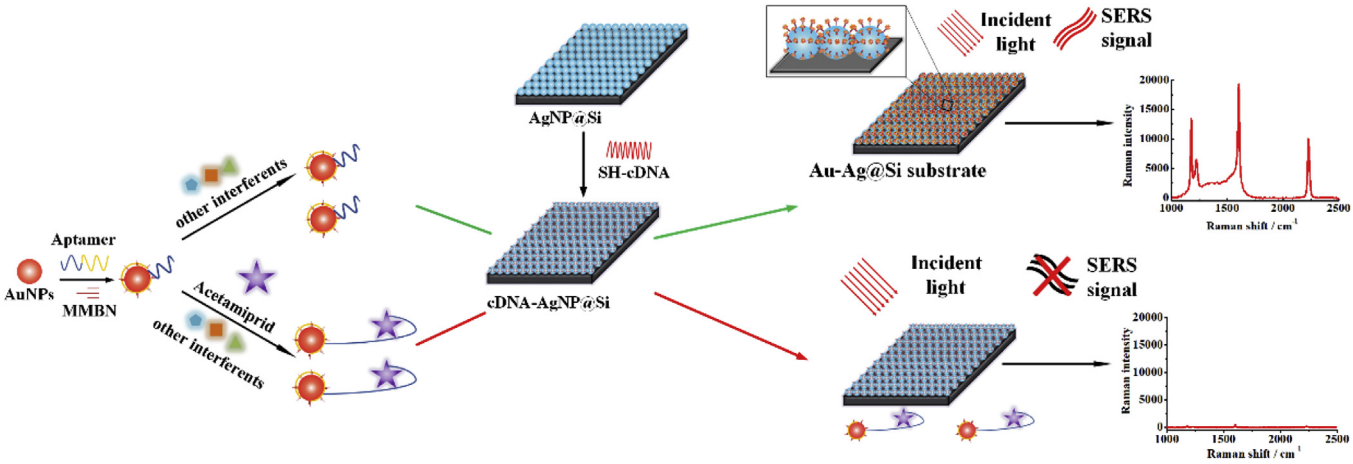

Scheme 1. Illustration of the fabrication process of aptasensor and mechanism for acetamiprid detection.

wafer covered by Si–H bonds. The modified Si wafer was immediately placed into the freshly prepared $AgNO_3$ solution with concentration of 5, 10, 20, 30, 40 and 50 mM for 90 s, producing AgNPs-deposited Si wafer (AgNPs@Si). Finally, the resultant AgNPs@Si substrate was dried with a gentle flow of nitrogen. The SERS performance of theses prepared AgNPs@Si substrates were featured by the enhancement factor (EF) value through incubating substrates with MMBN for 2 h. In detail, the EF value was calculated using the following equation (Zhu et al., 2015):

$$EF = \frac{I_{SERS} \times N_{bulk}}{I_{bulk} \times N_{SERS}} \quad (1)$$

Where, I_{SERS} and I_{bulk} were the intensity of the same Raman peak for the SERS and bulk Raman spectra, respectively. N_{bulk} was the number of bulk molecules probed in a bulk sample, and N_{SERS} was the number of molecules absorbed on the AgNPs@Si substrate.

2.4. Synthesis of AuNPs

AuNPs with the diameters of approximately 13 nm was synthesized by the citrate reduction methods (Grabar et al., 1995). Briefly, 100 mL of 1 mM boiling $HAuCl_4$ solution contained in 500 mL round-bottom flask was vigorously stirred. 10 mL of 60 mM sodium citrate was rapidly added into the vortexed solution and the condenser was quickly equipped. The color of the solution changed from pale yellow to burgundy. The system was allowed to remain boiling for another 20 min and then cooled to room temperature. The prepared AuNPs solution was stored at 4 °C in the refrigerator.

2.5. Establishment of acetamiprid SERS aptasensor system

The first step of establishing the acetamiprid SERS aptasensor system was to prepare the cDNA-AgNPs@Si substrate. The AgNPs deposited in previous prepared AgNPs@Si substrate as core nanoparticles were incubated with cDNA of different concentrations (250, 500, 750, 1000 and 1250 nM) in 10 mM phosphate-buffer saline (PBS) solution (pH 7.2) for 16 h. The substrate was then washed with 10 mM PBS solution (pH 7.2) three times and subsequently used as DNA anchoring.

The second step was to prepare the MMBN-AuNPs-aptamer mixture. 1 mL AuNPs solution was mixed with 10 μL MMBN of different concentrations (1, 2, 5 and 10 mM) to obtain AuNPs-MMBN solution. Then, 20 μL acetamiprid-binding aptamer of different concentrations (50, 100, 200, 300 and 400 nM) and AuNPs-MMBN solution were mixed and shaken for 1 min to obtain MMBN-AuNPs-aptamer hybrid. After that, citrate-HCl buffer (500 mM, pH 3.1) was quickly added to the above-mentioned solution to obtain a final citrate concentration of 10 mM, and then incubated for 60 min (Yao et al., 2015). Next, the excess aptamer was removed by centrifugation (12000 rpm, 15 min, 4 °C). The resultant solution was re-dissolved into 1 mL PBS solution and then was mixed with 20 μL acetamiprid solution of various concentration through shaking for 60 min. In a control experiment, 20 μL of ultrapure water was used in place of acetamiprid solution.

The final step was to prepare the Au-AgNPs@Si substrate. The prepared cDNA-AgNPs@Si substrate was immersed into the MMBN-AuNPs-aptamer mixture solution with different acetamiprid concentrations, and the mixture was incubated for 8 h. During this incubation process, if AuNPs with aptamer successfully captured acetamiprid, they would fail to connect with cDNA-AgNPs@Si substrate. Otherwise, MMBN-AuNPs-aptamer would bond with cDNA on the AgNPs@Si substrate to form the hybrid ("Au-AgNPs@Si"). Afterwards, the Au-AgNPs@Si substrate was washed with 10 mM PBS solution to remove the unconnected MMBN-AuNPs-aptamer, and then applied to perform the Raman intensity test. The Raman spectra in the wavelength range of 25–3558 cm^{-1} were recorded using Raman spectroscopy with a laser of 532 nm as excitation source and a power of 5 mW. The acquisition time was 1 s and the slit aperture was 50 μm. The other interferons were detected with the same method. SERS spectra and the intensities at 2227 cm^{-1} ($I_{2227\ cm\text{-}1}$) were recorded. Meanwhile, the blank substrate $(I_{2227\ cm\text{-}1})_0$ without acetamiprid was recorded, and the value of $\triangle I = (I_{2227\ cm\text{-}1})_0 - (I_{2227\ cm\text{-}1})$ was calculated.

2.6. Procedures for acetamiprid analysis in apple juice samples

The practical application of this proposed method for acetamiprid detection was evaluated by determining the recovery of experiment with standard addition method in apple juice samples. Fresh apple juice sample was prepared according to a previous literature with a slight simplification (Feng et al. (2017)). Briefly, 10 g apple tissue was sufficiently minced using a homogenizer with 10 mL water to produce apple juice. The obtained apple juice was filtered with a Whatman filter paper, and filtrate was centrifugated at 10000 rpm for 15 min. Finally, liquid supernatant was filtered through a 0.22 μm membrane syringe filter, and spiked with acetamiprid standard solution, resulting in artificial contamination at concentrations of 50, 100, 150 and 200 nM, respectively. The obtained apple juice samples were analyzed subsequently.

3. Results and discussion

3.1. Synthesis and characteristic of AgNPs@Si substrate

In this study, MMBN was used as a critical molecule to develop the suitable Raman tag with specific and stable signals, due to the following two reasons: First, nitrile group conjugating to aromatic ring could produce strong Raman signal because aromatic ring possesses relatively large Raman scattering cross section.; second, thiol group had high affinity to Au, which could ensure the successful connection of nitrile group with AuNPs. A previous literature showed that MMBN has been chosen as an excellent biomarker for protein imaging on the surface of cells, indicating its superiority of optical anti-interference in the presence of complex biomolecules (Kennedy et al., 2010). As shown in Fig. 1A, a prominent peak of Raman shift at ~2227 cm^{-1} could be observed owing to the stretch of C≡N bond. The sharp peak band at ~1601 cm^{-1} is assigned to the symmetric in-plane aromatic ring deformation, while the doublet at ~1221 cm^{-1} and ~1174 cm^{-1} is from the aromatic ring C–H deformation (Tay et al., 2010).

To test the optical anti-interference capability of nitrile, a comparison between MMBN and three conventional Raman tag molecules, namely malachite green (MG), methyl orange (MO) and rhodamine B (RB), was performed. Fig. S1A shows the Raman spectra of MG, MO, RB and MMBN. A number of peaks of these three conventional Raman tag molecules could be observed beyond the Raman-silent spectral window, and severely overlapped each other, while the nitrile in the MMBN displayed a distinct and sharp Raman scattering peak at 2227 cm^{-1}. To simplify the experiments, RB was selected as a representative of conventional Raman tags in the optical anti-interference ability test. As shown in Fig. S1B, when RB and the other three molecules (MG, MO and MMBN) were employed as the Raman tag (5 μM) and the organic interferences, respectively, the characteristic bands of RB (521, 621, 1280, 1358, 1509 and 1649 cm^{-1}) were severely masked by the peaks of MG, MO and MMBN. Meanwhile, this masking effect was aggravated with the increasing concentrations of the other interferences. The similar experimental phenomenon was also observed in a previous study (Zeng et al., 2016). By contrast, the characteristic peak (2227 cm^{-1}) of MMBN which served as the Raman tag remained highly distinguishable and stable in the presence of other interferences (RB, MG and MO) (Fig. S1C). The above results indicated that the MMBN molecule with nitrile was superior to the conventional Raman tags in terms of their optical anti-interference capabilities.

Immobilization of nanoparticles on solid substrates, such as silicon or glass support, could improve the reproducibility of Raman spectrum through reducing the random movement and aggregation of metal

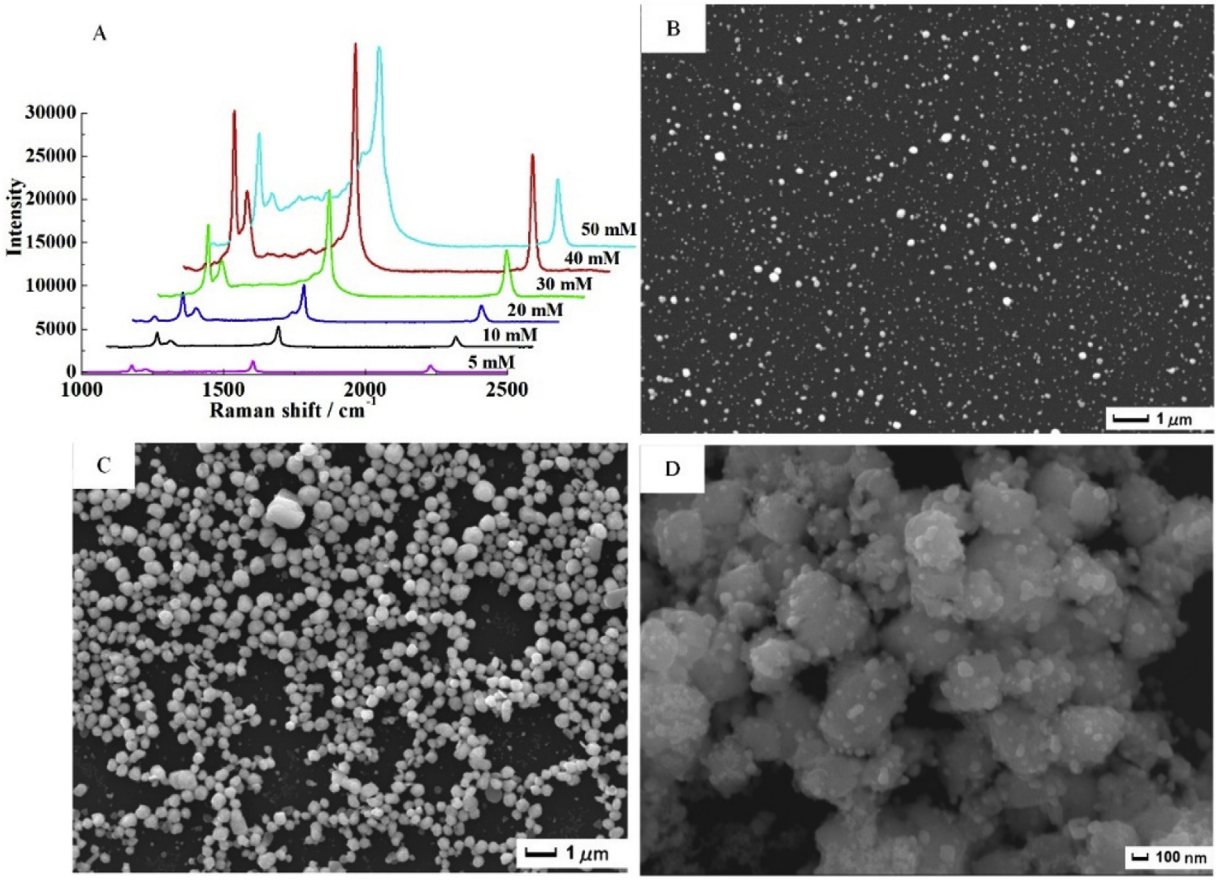

Fig. 1. (A) SERS spectra of 10^{-4} M MMBN deposited on six types of AgNP@Si substrate prepared at different concentration of $AgNO_3$. SEM images of AgNP@Si substrates prepared with $AgNO_3$ solution of (B) 10 mM, (C) 40 mM and (D) 50 mM.

nanoparticles caused by other interferences (Zhu et al., 2015). Therefore, the AgNPs was fabricated on the Si wafer substrate. The AgNPs@Si substrate was synthesized through in situ growth of AgNPs on silicon wafers according to the HF-etching method (Haldar et al., 2014). The influence of $AgNO_3$ solution concentration on the SERS performance of AgNPs@Si substrates and the morphology of silver nanoparticle on Si wafer was investigated. Fig. 1A shows the Raman signals of MMBN collected from six different SERS substrates prepared at different concentration of $AgNO_3$, while Fig. 1B–D presents the SEM images of AgNPs prepared with the increase of $AgNO_3$ concentration (10, 40 and 50 mM). At a low concentration of $AgNO_3$ (10 mM), the SERS intensity was weak (Fig. 1A). Meanwhile, the formed AgNPs had relatively small size (diameters less than 50 nm) and sparse distribution on silicon wafer (Fig. 1B). This was probably because on the surface of Si wafer, Ag^+ was firstly reduced to Ag forming silver agglomerates, but the crystal nuclei growth on the surface of silver agglomerates was too slow to form large sliver nanoparticles due to the low concentration of $AgNO_3$ (Wu et al., 2017). When elevating the concentration of $AgNO_3$ to 40 mM, AgNPs with large diameters and relatively spherical particle morphology were obtained (see Fig. 1C). The corresponding SERS intensity exhibited the highest value, indicating that the optimal $AgNO_3$ concentration was 40 mM to obtain an effective AgNPs@Si substrate. At a higher $AgNO_3$ concentration (50 mM), the Ag particles were fused onto the growing AgNPs surfaces (Fig. 1D), causing the stacking of these nanoparticles and the formation of irregular polygon silver nanoparticles. As a result, the corresponding Raman intensity decreased (Fig. 1A), implying the reducing of hot-spots on the AgNPs@Si substrate at such a high $AgNO_3$ concentration. Furthermore, the AgNPs@Si substrate prepared with 40 mM of $AgNO_3$ obtained the highest enhancement factor (EF) value of 5.08×10^5, which indicated that the Raman signal of MMBN was greatly amplified by the AgNPs@Si substrate. Hence, 40 mM was selected as the reasonable concentration of $AgNO_3$ solution to synthesize the AgNPs@Si substrate.

Subsequently, the resultant AgNPs@Si substrate was bonded with cDNA, and then incubated with aptamer to form the Au–AgNP@Si hybrid for acetamiprid detection.

3.2. Characterization of Au-AgNPs@Si hybrid

Firstly, the synthesized AuNPs were characterized by using UV–Vis spectra and TEM. As shown in Fig. S2A, a typical UV–Vis absorption peak appeared at ~520 nm, indicating the formation of AuNPs. The prepared AuNPs exhibited spherical structure (Fig. S2B), with an average diameter of 12.25 ± 1.25 nm (Fig. S2C) (calculated by 100 particles).

Then, the successful binding of MMBN on the surface of AuNPs was validated by Raman spectra shown in Fig. S3. As expected, the resultant AuNPs-MMBN exhibited distinct SERS signal of MMBN, while it did not appear in pure AuNPs.

Finally, as illustrated in Scheme 1, the AuNP-MMBN-aptamer could self-assemble with cDNA-AgNPs@Si substrate through hybridization between acetamiprid-binding aptamer and cDNA, to form Au-AgNPs@Si substrate. The low-magnification SEM images in Fig. 2A showed that the whole AgNPs were covered with a great number of AuNPs, indicating the successful fabrication of Au-AgNPs@Si substrate. This was also confirmed by the EDX spectroscopy that both Au and Ag elements co-existed in the hybrid structure (Fig. 2B). It is well known that SERS intensities are affected by the size of nanoparticles, so the use of 13 nm gold nanoparticles instead of ~300 nm silver nanoparticles as SERS substrate may result in a poorer enhancement effect (Li et al., 2017).

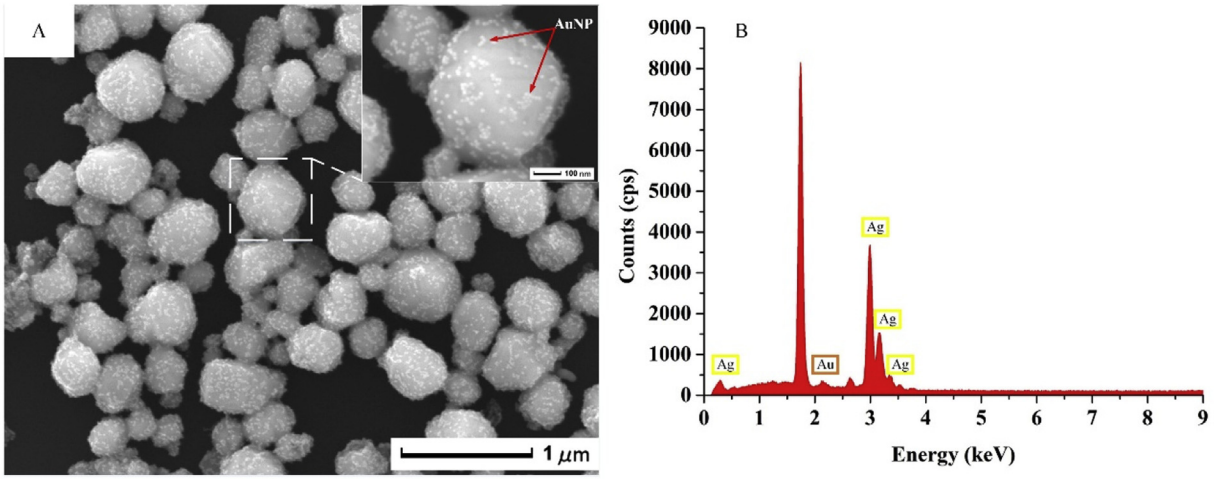

Fig. 2. (A) SEM images and (B) EDX spectroscopy to characterize Au-AgNPs@Si. Inset is the highly magnified SEM images of the Au-AgNPs@Si.

The experiment results in this study did show that the SERS performance of onefold AuNPs was not as good as Au–AgNP@Si (data not displayed). The high-magnification SEM image (Fig. 2A inset) also revealed that gold nanoparticles with homogeneous morphology randomly clustered on the surface of AgNPs. The clustering of nanoparticles was also responsible for high SERS activity. The nanogaps between AuNP and AgNP substrate can form hotspots to further enhance SERS signal, and the electromagnetic (EM) field distribution can also be deduced by three-dimensional finite-difference time-domain (3D-FDTD) simulation (Lumerical FDTD Solution, Inc., Canada). Fig. S4A-C show the theoretical simulation of EM filed spatial distribution for AuNP@Si, AgNP@Si and Au–AgNP@Si substrate, respectively. The plane wave source with the wavelength of 532 nm was selected and irradiated at normal incidence at the plasmon resonance frequency. As seen from Fig. S4A and B, the EM enhancement for AgNP was significantly higher than that for AuNP. Despite the obvious enhancement for AgNP, the gaps between adjacent nanoparticles (Au–Ag) provided more distinct SERS hot spots compared with the surface of bare AgNP (Fig. S4C). The local EM field enhancement in the gaps between Au–Ag was resulted from synergistic plasmonic enhancements effect (Cai et al., 2019). Therefore, these FDTD data essentially indicated that the fabricated Au–AgNP@Si could form excellent EM-field enhancement occurred at the junction of AuNP and AgNP, which made great contribution to superior enhancement of Raman signal.

3.3. Optimization of the Au-AgNPs@Si hybrid

To improve the sensitivity of aptasensor, three key parameters, namely cDNA concentration during preparation of cDNA-AgNPs@Si substrate, concentration of Raman tag (MMBN) and aptamer during the synthesis of AuNP-MMBN-aptamer hybrid, were optimized.

3.3.1. Effects of cDNA concentration

To evaluate the effect of cDNA concentration on SERS performance, cDNA with different concentrations was incubated with AgNPs@Si substrate, and then bonded with MMBN-AuNP-aptamer complex. The resulted peak intensity of each SERS spectrum was an average of 6 measurements. At a certain concentration of MMBN (10 mM) and aptamer (300 nM), the Raman intensity of MMBN at $\sim 2227\ cm^{-1}$ increased with the increase of cDNA concentration from 250 to 1000 nM, while it intended to decrease at a cDNA concentration of 1250 nM (Fig. 3A). The detailed Raman intensities at $\sim 2227\ cm^{-1}$ are shown in Fig. 3B. It can be seen that the Raman intensity of MMBN at a cDNA concentration of 1000 nM was nearly 5 times as high as that one at a cDNA concentration of 250 nM. As a consequence, 1000 nM cDNA was used for further study.

3.3.2. Effects of MMBN concentration

Fig. 3C–D shows that Raman intensity was enhanced with the increase of MMBN concentration and reached a plateau at 10 mM. However, when the concentration of MMBN rose to 15 mM, the color of AuNPs solution turned from wine-red to soft red, accompanied by obvious aggregation of AuNPs. More seriously, the AuNPs aggregation was largely adhered on the inner wall of tube after centrifugation and showed faint golden yellow color. The adverse aggregation could be due to that too much mercapto groups in MMBN reduced the electronegativity of AuNPs by replacing the citrate on the surface of AuNPs (Dong et al., 2017). Therefore, 10 mM of MMBN was selected as the proper reaction medium.

3.3.3. Effects of aptamer concentration

It can be seen from in Fig. 3E–F that the Raman intensity first rose and then declined when aptamer concentration increased up to 400 nM. The maximum Raman intensity was achieved at the aptamer concentration of 200 nM. Hence, the optimal aptamer concentration was experimentally determined to be 200 nM. According to a previous study (Yao et al., 2015), the sufficiently long polyA sequence in aptamer could wrap around the plane surface of AuNP, preventing further adsorption of additional strands. Namely, this polyA-mediated reaction suggested that the amount of aptamer attached onto AuNPs would reach saturation and no longer increase, even though the ratio of added aptamer to AuNPs increased. Hence, this confirmed that the optimal aptamer concentration was experimentally determined to be 200 nM.

3.4. SERS analysis of the acetamiprid by this aptasensor platform

Under the optimal experimental conditions, the response of aptasensor platform to acetamiprid with different concentration were determined. Fig. 4A shows that these was an inversely linear relationship between acetamiprid concentration and SERS signals intensity. Minus by the maximum SERS intensity at $2227\ cm^{-1}$ ($(I_{2227\ cm\text{-}1})_0$) when there was no acetamiprid, the linear relationship between SERS signal intensity difference $(I_{2227\ cm\text{-}1})_0$ - $(I_{2227\ cm\text{-}1})$ ($\triangle I$) and acetamiprid concentration was obtained in the range of 25–250 nM (Fig. 4B). The linearity correlation ($R^2 = 0.981$) was displayed in insert of Fig. 4B, and the limit of detection (LOD) was 6.8 nM at a signal-to-noise ratio of 3. Moreover, the analytical performance of this method was compared to various published methodologies recently, and the results were listed in Table 1. It was indicated that the proposed aptasensor possessed comparable LOD value to the reported methods.

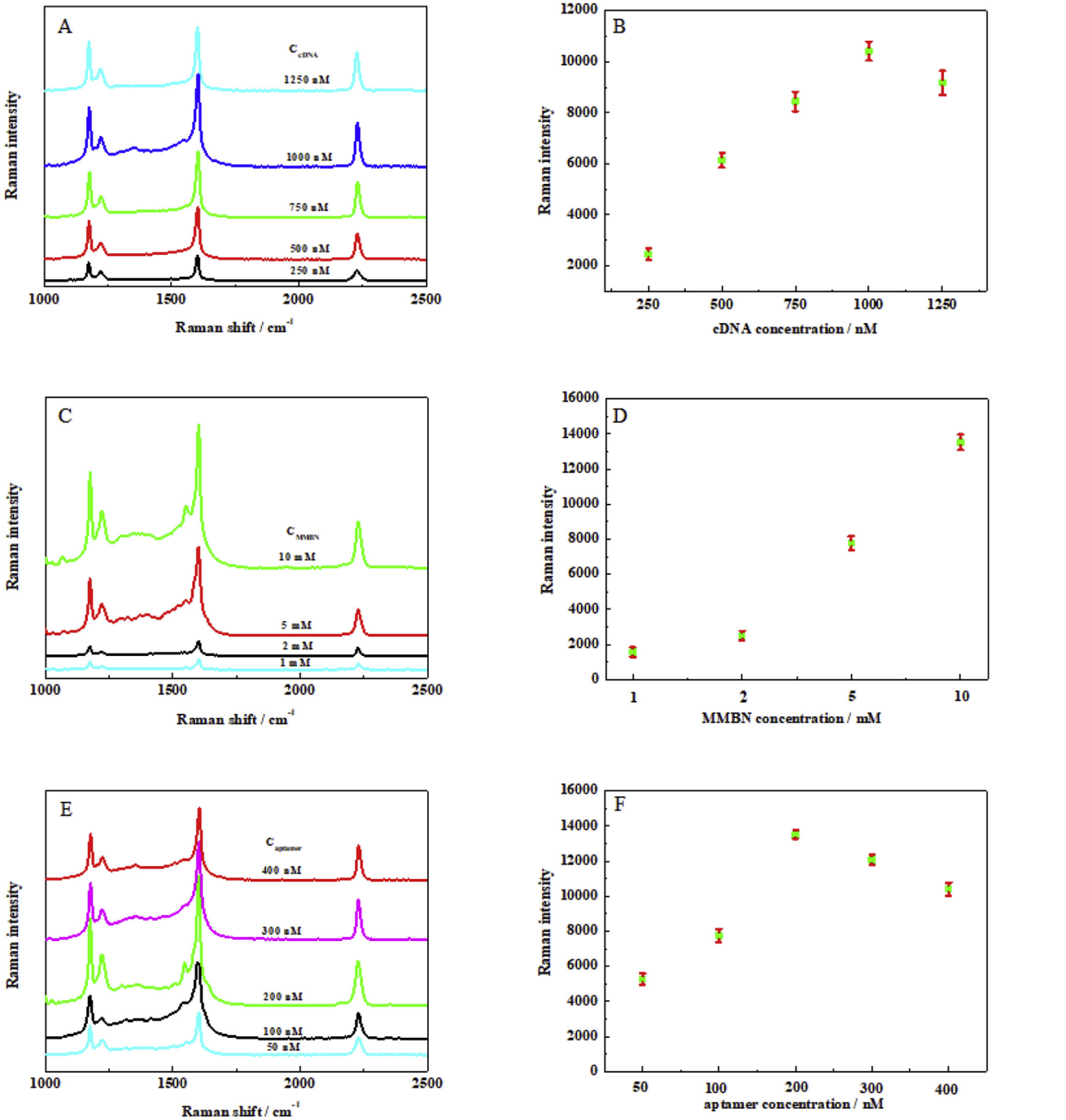

Fig. 3. Optimization of concentration of (A) cDNA, (C) MMBN, and (E) aptamer. SERS intensity detected at 2227 cm^{-1} for concentration of (B) cDNA, (D) MMBN, and (F) aptamer.

3.5. Selectivity, reproducibility and stability of the SERS aptasensor

Selectivity is an important property for the feasibility and practicability of the aptasensor platform. The selectivity of our aptasensor to the acetamiprid against other common pesticides, including imidacloprid, dichlorvos, phoxim, malathion and profenofos, were investigated. Fig. S5 illustrates that these pesticides did not make an obvious decrease of Raman intensity even if their concentration was 100 times as high as the concentration of acetamiprid under the same detection condition. This good selectivity of our aptasensor system was attributed to the specific bonding between the acetamiprid and the aptamer.

The reproducibility was also investigated by applying twenty different samples with the same acetamiprid concentration, and the corresponding Raman spectra were shown in Fig. S6. The relative standard deviation (RSD) of the Raman intensity at 2227 cm^{-1} was 3.47%, demonstrating the good reproducibility.

To investigate the stability of sensor for acetamiprid detection, AgNPs@Si substrate stored under nitrogen after one week or two weeks was used to fabricate the aptasensor. Fig. S7 shows that the intensity of SERS signal had no significant difference. Consequently, the developed aptasensor system could be a stable platform for the detection of acetamiprid.

3.6. Analysis of spiked apple juice samples

The content of acetamiprid in apple juice was measured to evaluate

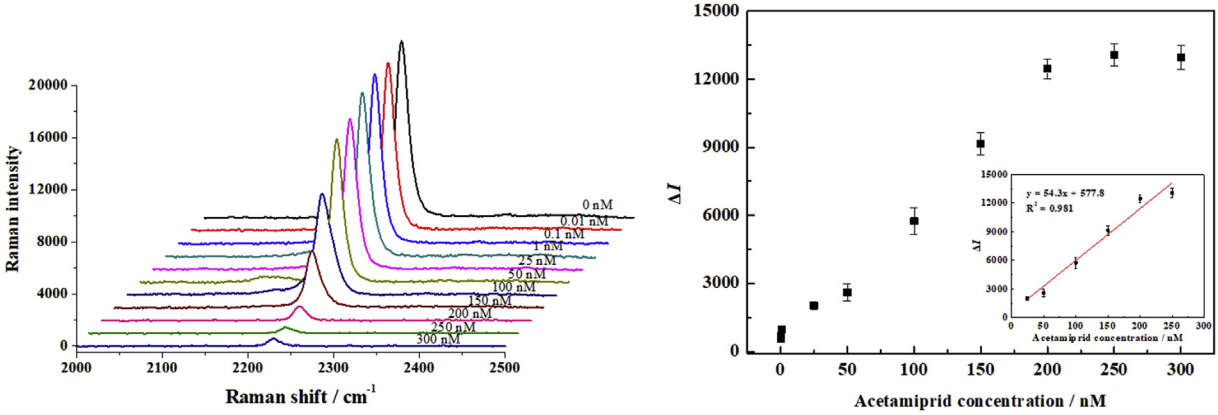

Fig. 4. (A) SERS spectra of MMBN for the detection of acetamiprid at different concentration. (B) SERS signal intensity difference at the peak of 2227 cm^{-1} ($\triangle I$) with the increase of acetamiprid concentration. Inset: linear calibration of $\triangle I$ value versus acetamiprid concentration.

Table 1
The comparison results of different aptasensors for acetamiprid detection.

Method	Linear range (*M*)	LOD (*M*)	References
Colorimetric	1×10^{-7}-1×10^{-5}	4×10^{-8}	Yang et al. (2015)
Fluorescent	1×10^{-7}-1.2×10^{-6}	9.12×10^{-9}	Liu et al. (2016)
Electrochemical	2.5×10^{-7}-2×10^{-6}	8.6×10^{-8}	Rapini et al. (2016)
Impedimetric	1×10^{-11}-1×10^{-7}	1×10^{-12}	Madianos et al. (2018)
SERS	4.50×10^{-10}-4.50×10^{-3}	9.59×10^{-11}	Hassan et al. (2019)
SERS	–	4.5×10^{-6}	Wei and Huang (2018)
SERS	2.5×10^{-8}-2.5×10^{-7}	6.8×10^{-9}	This work

the feasibility of this aptasensor for practical applications. Analytical results in Table S1 shows that the measured recoveries were in the range of 86.1%–100.3%, and RSD was less than 4.9%, suggesting that the established aptasensor can be applied to detect acetamiprid in real food samples.

4. Conclusion

In summary, a novel aptasensor system for acetamiprid detection has been developed using AuNP-MMBN-aptamer as the Raman probe, and cDNA-AgNPs@Si as the signal enhancer. The proposed Raman tag (MMBN) exhibited a highly distinguished, stable and strong signal at 2227 cm^{-1}. The aptasensor exhibited a linear detection range of 25–250 nM with a LOD of 6.8 nM to acetamiprid. Besides, the practicability of this method for acetamiprid detection in apple juice was also tested, and satisfactory recoveries were obtained. The results suggested that this developed SERS aptasensor could resist interferences in complex system and had great potential for trace detection of acetamiprid residues in foods.

CRediT authorship contribution statement

Yue Sun: Writing - original draft, Data curation. **Zhihua Li:** Conceptualization, Methodology. **Xiaowei Huang:** Resources, Formal analysis. **Di Zhang:** Data curation. **Xiaobo Zou:** Supervision, Project administration, Funding acquisition. **Jiyong Shi:** Funding acquisition. **Xiaodong Zhai:** Software, Writing - review & editing. **Caiping Jiang:** Investigation, Validation. **Xiaoou Wei:** Investigation, Writing - original draft, Writing - review & editing. **Tingting Liu:** Formal analysis.

Declaration of competing interest

The authors declare that they have no known competing financial interests or personal relationships that could have appeared to influence the work reported in this paper.

Acknowledgments

The authors gratefully acknowledge the financial support provided by the National Key Research and Development Program of China (2017YFC1600806, 2016YFD0401104), the National Natural Science Foundation of China (31801631, 31671844, 31601543), the Natural Science Foundation of Jiangsu Province (BK20160506, BE2016306, BK20180865), International Science and Technology Cooperation Project of Jiangsu Province (BZ2016013), and Priority Academic Program Development of Jiangsu Higher Education Institutions (PAPD).

Appendix A. Supplementary data

Supplementary data to this article can be found online at https://doi.org/10.1016/j.bios.2019.111672.

References

Albanito, L., Lappano, R., Madeo, A., Chimento, A., Prossnitz, E.R., Cappello, A.R., Dolce, V., Abonante, S., Pezzi, V., Maggiolini, M., 2008. G-protein-coupled receptor 30 and estrogen receptor-alpha are involved in the proliferative effects induced by atrazine in ovarian cancer cells. Environ. Health Perspect. 116 (12), 1648–1655.

Ando, J., Asanuma, M., Dodo, K., Yamakoshi, H., Kawata, S., Fujita, K., Sodeoka, M., 2016. Alkyne-tag SERS screening and identification of small-molecule-binding sites in protein. J. Am. Chem. Soc. 138 (42), 13901–13910.

Cai, Y., Huang, L., Wang, H., Dong, W., Zhang, Y., Zhang, W., Liu, Y., Li, G., Shang, F., Tong, H., 2019. Facile fabrication of 2D hetero core-satellites patterned Ag nanoparticle arrays with tunable plasmonic bands for SERS detection. Nanotechnology 30 (12) 125701.

Chen, Y., Ren, J.Q., Zhang, X.G., Wu, D.Y., Shen, A.G., Hu, J.M., 2016. Alkyne-modulated surface-enhanced Raman scattering-palette for optical interference-free and multiplex cellular imaging. Anal. Chem. 88 (12), 6115–6119.

Cheng, Z., Choi, N., Wang, R., Lee, S., Moon, K.C., Yoon, S.-Y., Chen, L., Choo, J., 2017. Simultaneous detection of dual prostate specific antigens using surface-enhanced Raman scattering-based immunoassay for accurate diagnosis of prostate cancer. ACS Nano 11 (5), 4926–4933.

Cooper, R.L., Laws, S.C., Das, P.C., Narotsky, M.G., Goldman, J.M., Lee Tyrey, E., Stoker, T.E., 2007. Atrazine and reproductive function: mode and mechanism of action studies. Birth Defects Res. Part B Dev. Reproductive Toxicol. 80 (2), 98–112.

Dao, T.C., Luong, T.Q.N., Cao, T.A., Kieu, N.M., Le, V.V., 2016. Application of silver nanodendrites deposited on silicon in SERS technique for the trace analysis of paraquat. Adv. Nat. Sci. Nanosci. Nanotechnol. 7 (1), 015007.
Dong, J.X., Gao, Z.F., Zhang, Y., Li, B.L., Li, N.B., Luo, H.Q., 2017. A selective and sensitive optical sensor for dissolved ammonia detection via agglomeration of fluorescent Ag nanoclusters and temperature gradient headspace single drop microextraction. Biosens. Bioelectron. 91, 155–161.
Feng, S., Hu, Y., Ma, L., Lu, X., 2017. Development of molecularly imprinted polymers-surface-enhanced Raman spectroscopy/colorimetric dual sensor for determination of chlorpyrifos in apple juice. Sens. Actuators B Chem. 241, 750–757.
Fu, C., Wang, Y., Chen, G., Yang, L., Xu, S., Xu, W., 2015. Aptamer-based surface-enhanced Raman scattering-microfluidic sensor for sensitive and selective polychlorinated biphenyls detection. Anal. Chem. 87 (19), 9555–9558.
Grabar, K.C., Freeman, R.G., Hommer, M.B., Natan, M.J., 1995. Preparation and characterization of Au colloid monolayers. Anal. Chem. 67 (4), 735–743.
Haldar, K.K., Kundu, S., Patra, A., 2014. Core-size-dependent catalytic properties of bimetallic Au/Ag core-shell nanoparticles. ACS Appl. Mater. Interfaces 6 (24), 21946–21953.
Han, C., Yao, Y., Wang, W., Qu, L., Bradley, L., Sun, S., Zhao, Y., 2017. Rapid and sensitive detection of sodium saccharin in soft drinks by silver nanorod array SERS substrates. Sens. Actuators B Chem. 251, 272–279.
Hassan, M.M., Chen, Q., Kutsanedzie, F.Y.H., Li, H., Zareef, M., Xu, Y., Yang, M., Agyekum, A.A., 2019. rGO-NS SERS-based coupled chemometric prediction of acetamiprid residue in green tea. J. Food Drug Anal. 27 (1), 145–153.
Hu, F., Zeng, C., Long, R., Miao, Y., Wei, L., Xu, Q., Min, W., 2018. Supermultiplexed optical imaging and barcoding with engineered polyynes. Nat. Methods 15 (3), 194–200.
Jamil, A.K.M., Izake, E.L., Sivanesan, A., Fredericks, P.M., 2015. Rapid detection of TNT in aqueous media by selective label free surface enhanced Raman spectroscopy. Talanta 134, 732–738.
Juan, D., Runping, W., Xiaoyue, X., Fuzhong, L., 2013. Research on the influencing factors of China apple juice trade. Res. J. Appl. Sci. Eng. Technol. 6 (4), 691–696.
Jung, J., Chen, L., Lee, S., Kim, S., Seong, G.H., Choo, J., Lee, E.K., Oh, C.-H., Lee, S., 2007. Fast and sensitive DNA analysis using changes in the FRET signals of molecular beacons in a PDMS microfluidic channel. Anal. Bioanal. Chem. 387 (8), 2609–2615.
Kennedy, D.C., Hoop, K.A., Tay, L.-L., Pezacki, J.P., 2010. Development of nanoparticle probes for multiplex SERS imaging of cell surface proteins. Nanoscale 2 (8), 1413–1416.
Kim, H.-J., Shelver, W.L., Li, Q.X., 2004. Monoclonal antibody-based enzyme-linked immunosorbent assay for the insecticide imidacloprid. Anal. Chim. Acta 509 (1), 111–118.
Li, D., Lv, D.Y., Zhu, Q.X., Li, H., Chen, H., Wu, M.M., Chai, Y.F., Lu, F., 2017. Chromatographic separation and detection of contaminants from whole milk powder using a chitosan-modified silver nanoparticles surface-enhanced Raman scattering device. Food Chem. 224, 382–389.
Li, D.W., Qu, L.L., Hu, K., Long, Y.T., Tian, H., 2015a. Monitoring of endogenous hydrogen sulfide in living cells using surface-enhanced Raman scattering. Angew. Chem. Int. Ed. 54 (43), 12758–12761.
Li, S., Xu, L., Ma, W., Kuang, H., Wang, L., Xu, C., 2015b. Triple Raman label-encoded gold nanoparticle trimers for simultaneous heavy metal ion detection. Small 11 (28), 3435–3439.
Liu, H., Yang, L., Ma, H., Qi, Z., Liu, J., 2011. Molecular sensitivity of DNA–Ag–PATP hybrid on optical activity for ultratrace mercury analysis. Chem. Commun. 47 (33), 9360–9362.
Liu, X., Li, Y., Liang, J., Zhu, W., Xu, J., Su, R., Yuan, L., Sun, C., 2016. Aptamer contained triple-helix molecular switch for rapid fluorescent sensing of acetamiprid. Talanta 160, 99–105.
Madianos, L., Tsekenis, G., Skotadis, E., Patsiouras, L., Tsoukalas, D., 2018. A highly sensitive impedimetric aptasensor for the selective detection of acetamiprid and atrazine based on microwires formed by platinum nanoparticles. Biosens. Bioelectron. 101, 268–274.
Park, J.-Y., Choi, J.-H., Kim, B.-M., Park, J.-H., Cho, S.-K., Ghafar, M.W., Abd El-Aty, A.M., Shim, J.-H., 2011. Determination of acetamiprid residues in zucchini grown under greenhouse conditions: application to behavioral dynamics. Biomed. Chromatogr. 25 (1-2), 136–146.
Pramanik, S.K., Bhattacharyya, J., Dutta, S., Dey, P.K., Bhattacharyya, A., 2006. Persistence of acetamiprid in/on mustard (Brassica juncea L.). Bull. Environ. Contam. Toxicol. 76 (2), 356–360.
Rapini, R., Cincinelli, A., Marrazza, G., 2016. Acetamiprid multidetection by disposable electrochemical DNA aptasensor. Talanta 161, 15–21.
Renaud, M., Akeju, T., Natal-da-Luz, T., Leston, S., Rosa, J., Ramos, F., Sousa, J.P., Azevedo-Pereira, H.M.V.S., 2018. Effects of the neonicotinoids acetamiprid and thiacloprid in their commercial formulations on soil fauna. Chemosphere 194, 85–93.
Sanyal, D., Chakma, D., Alam, S., 2008. Persistence of a neonicotinoid insecticide, acetamiprid on chili (capsicum annum L.). Bull. Environ. Contam. Toxicol. 81 (4), 365–368.
Sun, F., Ella-Menye, J.R., Galvan, D.D., Bai, T., Hung, H.C., Chou, Y.N., Zhang, P., Jiang, S., Yu, Q., 2015. Stealth surface modification of surface-enhanced Raman scattering substrates for sensitive and accurate detection in protein solutions. ACS Nano 9 (3), 2668–2676.
Tay, L.-L., Hulse, J., Kennedy, D., Pezacki, J.P., 2010. Surface-enhanced Raman and resonant Rayleigh scatterings from adsorbate saturated nanoparticles. J. Phys. Chem. C 114 (16), 7356–7363.
Tchounwou, P.B., Wilson, B.A., Ishaque, A.B., Schneider, J., 2001. Atrazine potentiation of arsenic trioxide-induced cytotoxicity and gene expression in human liver carcinoma cells (HepG2). Mol. Cell. Biochem. 222 (1), 49–59.
Wang, G., Wang, Y., Chen, L., Choo, J., 2010. Nanomaterial-assisted aptamers for optical sensing. Biosens. Bioelectron. 25 (8), 1859–1868.
Wang, W., Ding, X., He, M., Wang, J., Lou, X., 2014. Kinetic adsorption profile and conformation evolution at the DNA-gold nanoparticle interface probed by dynamic light scattering. Anal. Chem. 86 (20), 10186–10192.
Wang, Y., Yan, B., Chen, L., 2013. SERS tags: novel optical nanoprobes for bioanalysis. Chem. Rev. 113 (3), 1391–1428.
Wei, L., Hu, F., Shen, Y., Chen, Z., Yu, Y., Lin, C.C., Wang, M.C., Min, W., 2014. Live-cell imaging of alkyne-tagged small biomolecules by stimulated Raman scattering. Nat. Methods 11 (4), 410–412.
Wei, W., Huang, Q., 2018. Preparation of cellophane-based substrate and its SERS performance on the detection of CV and acetamiprid. Spectrochim. Acta A Mol. Biomol. Spectrosc. 193, 8–13.
Wu, Y.X., Liang, P., Dong, Q.M., Bai, Y., Yu, Z., Huang, J., Zhong, Y., Dai, Y.C., Ni, D., Shu, H.B., Pittman Jr., C.U., 2017. Design of a silver nanoparticle for sensitive surface enhanced Raman spectroscopy detection of carmine dye. Food Chem. 237, 974–980.
Xie, W., Han, C., Qian, Y., Ding, H., Chen, X., Xi, J., 2011. Determination of neonicotinoid pesticides residues in agricultural samples by solid-phase extraction combined with liquid chromatography–tandem mass spectrometry. J. Chromatogr. A 1218 (28), 4426–4433.
Yamakoshi, H., Dodo, K., Okada, M., Ando, J., Palonpon, A., Fujita, K., Kawata, S., Sodeoka, M., 2011. Imaging of EdU, an alkyne-tagged cell proliferation probe, by Raman microscopy. J. Am. Chem. Soc. 133 (16), 6102–6105.
Yamakoshi, H., Dodo, K., Palonpon, A., Ando, J., Fujita, K., Kawata, S., Sodeoka, M., 2012. Alkyne-tag Raman imaging for visualization of mobile small molecules in live cells. J. Am. Chem. Soc. 134 (51), 20681–20689.
Yang, Z., Qian, J., Yang, X., Jiang, D., Du, X., Wang, K., Mao, H., Wang, K., 2015. A facile label-free colorimetric aptasensor for acetamiprid based on the peroxidase-like activity of hemin-functionalized reduced graphene oxide. Biosens. Bioelectron. 65, 39–46.
Yao, G., Pei, H., Li, J., Zhao, Y., Zhu, D., Zhang, Y., Lin, Y., Huang, Q., Fan, C., 2015. Clicking DNA to gold nanoparticles: poly-adenine-mediated formation of monovalent DNA-gold nanoparticle conjugates with nearly quantitative yield. NPG Asia Mater. 7 (1) e159-e159.
Zeng, Y., Ren, J., Shen, A., Hu, J., 2016. Field and pretreatment-free detection of heavy-metal ions in organic polluted water through an alkyne-coded SERS test kit. ACS Appl. Mater. Interfaces 8 (41), 27772–27778.
Zhang, B., Pan, X., Venne, L., Dunnum, S., McMurry, S.T., Cobb, G.P., Anderson, T.A., 2008. Development of a method for the determination of 9 currently used cotton pesticides by gas chromatography with electron capture detection. Talanta 75 (4), 1055–1060.
Zhang, J., Liang, L., Guan, X., Deng, R., Qu, H., Huang, D., Xu, S., Liang, C., Xu, W., 2018. In situ, accurate, surface-enhanced Raman scattering detection of cancer cell nucleus with synchronous location by an alkyne-labeled biomolecular probe. Anal. Bioanal. Chem. 410 (2), 585–594.
Zhao, B., Shen, J., Chen, S., Wang, D., Li, F., Mathur, S., Song, S., Fan, C., 2014. Gold nanostructures encoded by non-fluorescent small molecules in polyA-mediated nanogaps as universal SERS nanotags for recognizing various bioactive molecules. Chem. Sci. 5 (11), 4460–4466.
Zhu, Y., Jiang, X., Wang, H., Wang, S., Wang, H., Sun, B., Su, Y., He, Y., 2015. A poly adenine-mediated assembly strategy for designing surface-enhanced resonance Raman scattering substrates in controllable manners. Anal. Chem. 87 (13), 6631–6638.